

# Diversity of Fuzzy Dark Matter Solitons

Chen Tan<sup>1,2,3,4</sup>, M. Le Delliou<sup>1,2,3,4,5,6</sup>, and Ke Wang<sup>7\*</sup>

<sup>1</sup>*School of Physical Science and Technology, Lanzhou University, Lanzhou 730000, China*

<sup>2</sup>*Institute of Theoretical Physics & Research Center of Gravitation, Lanzhou University, Lanzhou 730000, China*

<sup>3</sup>*Key Laboratory of Quantum Theory and Applications of MoE, Lanzhou University, Lanzhou 730000, China*

<sup>4</sup>*Lanzhou Center for Theoretical Physics & Key Laboratory of Theoretical Physics of Gansu Province, Lanzhou University, Lanzhou 730000, China*

<sup>5</sup>*Instituto de Astrofísica e Ciências do Espaço, Universidade de Lisboa, Faculdade de Ciências, Ed. C8, Campo Grande, 1769-016 Lisboa, Portugal*

<sup>6</sup>*Université de Paris-Cité, APC-Astroparticule et Cosmologie (UMR-CNRS 7164), F-75006 Paris, France and*

<sup>7</sup>*Department of Physics, Liaoning Normal University, Dalian 116029, China*

(Dated: August 29, 2025)

According to the Schrödinger-Poisson equations, fuzzy dark matter (FDM) can form a stable equilibrium configuration, the so-called FDM soliton. In principle, given the FDM particle mass, the profile of the FDM soliton is fixed. In practice, however, there is a great diversity of structures in the Universe. Possible causes of such diversity can lie in such sources as the gravitoelectric field due to a central supermassive black hole, the gravitomagnetic field due to the system angular momentum, an extra denser and compact FDM soliton and an ellipsoidal baryon background. We find that the effects of the gravitomagnetic field due to the soliton's self-angular momentum are very weak while those of the other sources are considerable.

## I. INTRODUCTION

The existence of dark matter (DM) is strongly suggested from rotation curves of galaxies [1], evolution of large scale structure [2] and gravitational lensing observations [3]. Depending on the free streaming length of DM, it can be divided into cold, warm and hot categories. Although the standard Lambda cold DM ( $\Lambda$ CDM) cosmological model is very successful and the latest cosmic microwave background (CMB) observations [4] suggests that CDM accounts for about 26% of today's energy density in the Universe, we still have no certainty on the existence or nature of CDM, whether sourced by particles, other objects or explained away by gravity modifications [5]. Especially, as one of the most promising candidates for CDM particle, the weakly interacting massive particles (WIMPs) grounded on supersymmetric theories of particle physics still have not been detected [6–8]. Moreover, primordial black holes (BHs) can also serve as CDM [9], although they still have not been identified. These null results coupled with the failures of CDM particles on sub-galactic scales [10, 11] imply that DM may not entirely fall under the CDM paradigm.

A promising alternative to CDM lies in an ultralight scalar field with spin-0, extraordinarily light mass ( $\sim 10^{-22}\text{eV}/c^2$ ) and de Broglie wavelength comparable to a few kpc, coined fuzzy DM (FDM) [12]. Due to its large occupation numbers in galactic halos, FDM behaves as a classical field obeying the coupled Schrödinger–Poisson

(SP) system of equations,

$$\begin{cases} i\hbar\frac{\partial\Psi}{\partial t} = \left(-\frac{\hbar^2}{2m}\nabla^2 + m\Phi\right)\Psi, \\ \nabla^2\Phi = 4\pi G|\Psi|^2, \end{cases} \quad (1)$$

where  $m$  is the mass of the FDM particle, which is described by the wavefunction  $\Psi$ , and the gravitational potential  $\Phi$  is sourced by the FDM density  $\rho = |\Psi|^2$ . According to Eq. (1), FDM can condensate into a many particles ground state coined as soliton. The SP system can also describe the evolution of FDM in an expanding Universe [13–16]. Note that the SP system is just the weak field limit of the general relativistic Einstein–Klein–Gordon (EKG) system [17–19] and that the SP system should be replaced by the Gross-Pitaevskii-Poisson (GPP) system when FDM particles self-interactions exist [20, 21].

In this paper, for simplicity, we confine ourself to the SP system in a non-expanding Universe. The evolution of this system is usually simulated numerically, including the formation, perturbation, interference/collision and tidal disruption/deformation of FDM solitons [22–25]. Focussing on stationary solutions, one can turn to the shooting method to compute the eigenvalues of equilibrium configurations [22, 26]. In this work we restrict to different situations where numerical treatment can be avoided cleverly, as illustrated below.

Since FDM solitons only depend on the mass of FDM, the SP system obeys scaling symmetry. As a result, the Universe should *a priori* present very monotonous and similar structures. Yet, there is a great diversity of structures in the Universe. Therefore, although we do not here consider the modifications of gravity or various possible FDM interactions, the real astrophysics systems must follow variants of the exact SP system. In this paper, we will consider several variants, induced by extra terms, such as

\*Corresponding author: wangke@lnnu.edu.cn

the gravitoelectric field, the gravitomagnetic field, both sourced by the Weyl tensor [27], an extra FDM soliton and the baryon density profile. Our motivations are as follows. First since, as pointed out in [22, 28], the SP system is the weak field limit of the EKG system, there must exist a variant system, between these two systems, for which gravitoelectromagnetism is a good approximation. While the gravitoelectric field or the gravitational potential of a supermassive BH has been discussed [24–26], the gravitomagnetic field due to the system’s angular momentum has not yet been considered. Secondly, although the interference/collision with an extra FDM soliton has also been studied [23–25], those studies restricted to the cases in which the density-ratio of two solitons is  $\sim 1$ . For the extreme cases where the density-ratio of the denser solitons to another one is  $\gtrsim 10^4$ , numerical simulations would require a large enough simulation box to contain the larger soliton with lower density, while requiring a higher resolution to depict the smaller soliton with higher density. However, a simulation combining a large simulation box and high resolution at the same time is prohibitively expensive and almost impossible to solve. Finally, when non-spherical baryon profile is located in galaxies, it results in non-spherical FDM solitons. The impact of a baryon profile with cylindrical symmetry has been quantified in [29]. In fact, the baryon profile in the Milky Way may be ellipsoidal [30, 31].

This paper is organized as follows. In section II, we briefly review the effects of the gravitoelectric field due to a supermassive BH on the FDM solitons. In section III, we study the effects of the gravitomagnetic field due to the rotation velocity of FDM, the supermassive BH spin and the orbital motion of supermassive BH binary on the FDM solitons. In section IV, we study the interaction between soliton binary with the extreme density-ratio. In section V, we calculate the FDM solitons in a given ellipsoidal baryon profile. Finally, a brief summary and discussions are included in section VI.

## II. EFFECTS OF THE GRAVITOELECTRIC FIELD

The effects of the gravitoelectric field include the tidal disruption/deformation of FDM solitons by a nearby supermassive BH [24, 25] and the modified formation of FDM solitons by a central supermassive BH [26]. While the former non-spherical impacts are more complicated and have to be studied by numerical simulations, the latter spherical ones are simple and can be studied by the shooting method. In this section, we briefly review the latter cases.

Firstly, the gravitoelectric field  $\mathbf{E}_g$  derived from the gravitational potential  $\Phi_e$ , sourced by a central supermassive BH, contributes to a variant of the exact SP

system as

$$\begin{cases} i\hbar \frac{\partial \Psi}{\partial t} = \left[ -\frac{\hbar^2}{2m} \nabla^2 + m(\Phi + \Phi_e) \right] \Psi, \\ \nabla^2 \Phi = 4\pi G |\Psi|^2, \end{cases} \quad (2)$$

where the supermassive BH with mass  $M_{bh}$  has a point mass potential

$$\Phi_e = -\frac{GM_{bh}}{r}. \quad (3)$$

When the system in question features spherical symmetry, the ansatz of  $\Psi(r, t) = e^{-i\gamma t/\hbar} \psi(r)$ , where  $\gamma$  can be interpreted as the ansatz energy eigenvalue, leads to the FDM soliton density  $\rho(r) = |\Psi|^2 = \psi^2(r)$  and the FDM soliton mass  $M = \int_0^\infty 4\pi r^2 \rho(r) dr$ . After defining the system’s dimensionless variables as

$$\tilde{\psi} \equiv \frac{\hbar \sqrt{4\pi G}}{mc^2} \psi, \quad (4)$$

$$\tilde{r} \equiv \frac{mc}{\hbar} r, \quad (5)$$

$$\tilde{\Phi} \equiv \frac{1}{c^2} \Phi, \quad (6)$$

$$\tilde{\gamma} \equiv \frac{1}{mc^2} \gamma, \quad (7)$$

$$\tilde{M} \equiv \frac{GMm}{\hbar c}, \quad (8)$$

$$\tilde{M}_{bh} \equiv \frac{GM_{bh}m}{\hbar c}, \quad (9)$$

the dimensionless version of Eq. (2), with the spherical ansatz, follows

$$\begin{cases} \frac{\partial^2(\tilde{r}\tilde{\psi})}{\partial \tilde{r}^2} = 2\tilde{r} \left( \tilde{\Phi} - \tilde{\gamma} - \frac{\tilde{M}_{bh}}{\tilde{r}} \right) \tilde{\psi}, \\ \frac{\partial^2(\tilde{r}\tilde{\Phi})}{\partial \tilde{r}^2} = \tilde{r}\tilde{\psi}^2. \end{cases} \quad (10)$$

Fulfilling the arbitrary normalization  $\tilde{\psi}(\tilde{r} = 0) = 1$  and  $\tilde{\Phi}(\tilde{r} = 0) = 0^1$ , the boundary conditions  $\tilde{\psi}(\tilde{r} = \infty) = 0$ ,  $\frac{\partial \tilde{\psi}}{\partial \tilde{r}}|_{\tilde{r}=0} = 0$  and  $\frac{\partial \tilde{\Phi}}{\partial \tilde{r}}|_{\tilde{r}=0} = 0$ , choosing the supermassive BH mass  $\tilde{M}_{bh} = \{0.0, 0.5, 1.0, 1.5, 2.0, 2, 5\}$  as the input parameter and adjusting the quantized eigenvalue  $\tilde{\gamma}$ , we can calculate the equilibrium configurations from Eq. (10) by the shooting method. Given the input parameter  $\tilde{M}_{bh}$ , we obtain the only stable solution from the smallest  $\tilde{\gamma}$ , which is the ground state. In Tab. I,

<sup>1</sup> This normalization condition for the soliton self-potential,  $\Phi$ , is different from the conventional choice of normalization as for the BH potential,  $\Phi_e$ , that  $\Phi_e(r = \infty) = 0$ . Although it produces a nonvanishing asymptotic value at infinity,  $\tilde{\Phi}(\tilde{r} = \infty)$ , this difference does not affect the solutions with the normalization  $\tilde{\psi}(\tilde{r} = 0) = 1$ .

we list the input values of  $\tilde{M}_{\text{bh}}$  and the corresponding eigenvalue  $\tilde{\gamma}$  and soliton mass  $\tilde{M}$  of the ground state solutions. In Fig. 1, the corresponding soliton profiles are plotted. We find that the larger  $\tilde{M}_{\text{bh}}$  results in a denser and more compact soliton, leading to a smaller dimensionless soliton mass  $\tilde{M}$ , due to the fixed normalization  $\tilde{\psi}(\tilde{r} = 0) = 1$ . The solutions under this normalization can be rescaled by the following scaling symmetry

$$\tilde{\psi} \longrightarrow \lambda \tilde{\psi}, \quad (11)$$

$$\tilde{r} \longrightarrow \lambda^{-1/2} \tilde{r}, \quad (12)$$

$$\tilde{\Phi} \longrightarrow \lambda \tilde{\Phi}, \quad (13)$$

$$\tilde{\gamma} \longrightarrow \lambda \tilde{\gamma}, \quad (14)$$

$$\tilde{M} \longrightarrow \lambda^{1/2} \tilde{M}, \quad (15)$$

$$\tilde{M}_{\text{bh}} \longrightarrow \lambda^{1/2} \tilde{M}_{\text{bh}}. \quad (16)$$

Taking into account a simultaneously increasing  $\lambda$ , the physical mass  $M$  actually increases with  $\tilde{M}_{\text{bh}}$  [26].

TABLE I: Input values of the dimensionless supermassive BH mass  $\tilde{M}_{\text{bh}}$  and the corresponding eigenvalue  $\tilde{\gamma}$  and soliton dimensionless mass  $\tilde{M}$  of the ground state solutions.

$\tilde{M}_{\text{bh}}$	$\tilde{\gamma}$	$\tilde{M}$
0.0	0.6495	2.0622
0.5	0.1164	0.7916
1.0	-0.5113	0.2169
1.5	-1.0839	0.0718
2.0	-1.9767	0.0309
2.5	-3.1101	0.0159

### III. EFFECTS OF THE GRAVITOMAGNETIC FIELD

The SP system corresponds to the weak field limit of the general relativistic EKG system [22]. A variant system can therefore account for some general relativistic corrections to the SP system, on the spectrum between the full EKG system and its weak field approximation, such as the gravitomagnetic field  $\mathbf{B}_g$ . Such variant of the exact SP system reads

$$\begin{cases} i\hbar \frac{\partial \Psi}{\partial t} = \left[ -\frac{\hbar^2}{2m} \nabla^2 + m(\Phi + \Phi_e + \Phi_m) \right] \Psi, \\ \nabla^2 \Phi = 4\pi G |\Psi|^2, \end{cases} \quad (17)$$

where the gravitational potential  $\Phi_m$  is related to the gravitomagnetic field  $\mathbf{B}_g$  and the angular momentum<sup>2</sup> of

an FDM particle  $\hat{\mathbf{L}}$ . In the case of a non-uniform gravitomagnetic field, we should use the following expression, in analogy to the effect of an external magnetic field in non-relativistic quantum mechanics,

$$\begin{aligned} \Phi_m &= \Phi_{m1} + \Phi_{m2} \\ &= \frac{i\hbar}{m} \mathbf{A}_g \cdot \nabla + \frac{1}{2} \mathbf{A}_g \cdot \mathbf{A}_g, \end{aligned} \quad (18)$$

where  $\mathbf{A}_g$  is the gravitomagnetic vector potential, related to the gravitomagnetic field as  $\mathbf{B}_g = \nabla \times \mathbf{A}_g$ . For the vector potential component in the azimuthal angular direction  $\partial_\phi$ , it takes the form

$$\Phi_m = -\frac{1}{mr} A_g^\phi \hat{L}_z + \frac{1}{2} A_g^\phi A_g^\phi. \quad (19)$$

Generally speaking, the linear term  $\Phi_{m1}$  is much larger than the quadratic one  $\Phi_{m2}$ . In this section, we will talk about some possible sources of  $\mathbf{A}_g$  and their effects on the FDM solitons.

#### A. Gravitomagnetic field due to rotation velocity of fuzzy dark matter

The gravitational potential inside an FDM soliton sourced by its own density profile follows the spherically symmetric potential

$$\Phi = -\frac{4\pi G \int_0^r \rho(R) R^2 dR}{r} - 4\pi G \int_r^\infty \frac{\rho(R) R^2 dR}{R}, \quad (20)$$

where we temporarily utilize the normalization  $\Phi(r = \infty) = 0$  in Sec. III, as we did not solve the SP system but rather estimate and compare the effect of different potentials. If this FDM soliton is rotating around the  $z$ -axis, there should be a non-zero  $A_g^\phi$  in the  $x-y$  plane according to gravitoelectromagnetism. To calculate the total  $A_g^\phi$  in the  $x-y$  plane, inside the FDM soliton, we first consider an FDM density shell with radius  $R$  rotating around the  $z$ -axis with a typical linear velocity, in the  $x-y$  plane, relative to the FDM soliton's center  $v \sim 10^{-3}c$ . The infinitesimal  $dA_g^\phi$  in the  $x-y$  plane produced by this FDM spherical shell verifies

$$dA_g^\phi = \begin{cases} -\frac{4\pi G v \rho(R) R^3 dR}{3c^2 r^2}, & (r > R), \\ -\frac{4\pi G}{3c^2} v \rho(R) r dR, & (r < R). \end{cases} \quad (21)$$

particles in the soliton. As  $N$  is constant, we have  $i\hbar \frac{\partial \Psi}{\partial t} = i\hbar \frac{\partial \sqrt{N} \Psi_1}{\partial t} = \sqrt{N} i\hbar \frac{\partial \Psi_1}{\partial t}$ . Therefore the Schrödinger Eq. (17) can reduce to the description of a single particle of the soliton and the  $\hat{\mathbf{L}}$  operator brings out the angular momentum for a single particle.

<sup>2</sup> Note that  $\Psi = \sqrt{N} \Psi_1$  [18], where  $\Psi_1$  is the dimensional wavefunction of one FDM particle and  $N$  is the fixed number of

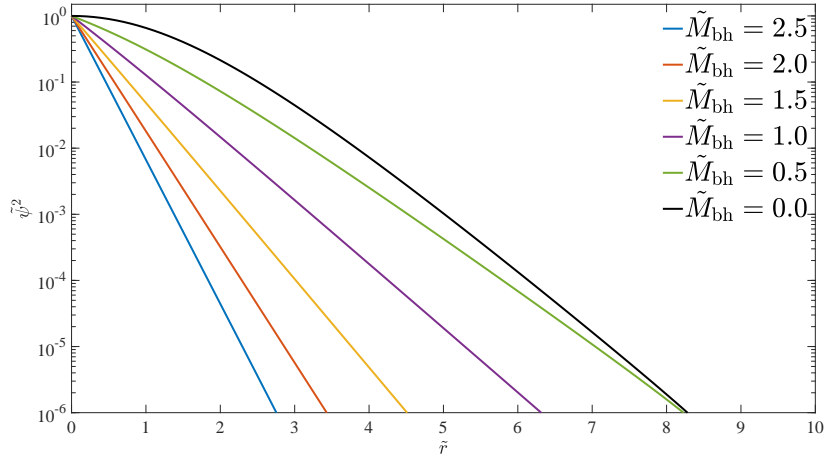


FIG. 1: Density profiles of the ground state solutions with different dimensionless supermassive BH mass  $\tilde{M}_{bh}$ .

Then the total  $A_g^\phi$  produced by the whole FDM soliton sums up to

$$\begin{aligned} A_g^\phi &= -\frac{4\pi Gv}{3c^2} \left( \frac{1}{r^2} \int_0^r \rho(R) R^2 dR + r \int_r^\infty \rho(R) dR \right) \\ &= \frac{4\pi Gv}{3c^2} f(r), \end{aligned} \quad (22)$$

where the density  $\rho$  is rescaled from the dimensionless density of the black curve in Fig. 1. The scaling factor  $\lambda$  is determined from the comparison between the integration of the black curve and a given soliton mass  $M$ . The soliton mass  $M$  can be predicted from the halo mass  $M_{halo}$  according to the soliton-halo mass relation, whether from the version of Ref. [14]

$$M \approx 1.25 \times 10^9 \left( \frac{M_{halo}}{10^{12} M_\odot} \right)^{1/3} \left( \frac{m}{10^{-22} \text{eV}/c^2} \right)^{-1} M_\odot, \quad (23)$$

or following the version of Ref. [32]

$$\begin{aligned} M \approx & \beta \left( \frac{m}{8 \times 10^{-23} \text{eV}/c^2} \right)^{-3/2} \\ & + \left( \frac{M_{halo}}{\gamma} \right)^\alpha \left( \frac{m}{8 \times 10^{-23} \text{eV}/c^2} \right)^{3(\alpha-1)/2} M_\odot, \end{aligned} \quad (24)$$

where  $\beta = 8.00 \times 10^6 M_\odot$ ,  $\gamma = 10^{-5.73} M_\odot$  and  $\alpha = 0.515$ . The following discussion takes the Milky Way value with  $M_{halo} = 1 \times 10^{12} M_\odot$  [33] as an example.

The angular momentum of each particle of the soliton being identical, and in the  $z$  direction, we compute its magnitude by dividing the FDM shells angular momentum, integrated over the soliton, by the number of FDM particles in the soliton  $N = M/m$ , according to

$$L_z = \frac{1}{N} \int_0^\infty \frac{8\pi}{3} \rho(R) R^3 v dR. \quad (25)$$

According to Eq. (19), the linear gravitational potential in the  $x-y$  plane yields

$$\Phi_{m1} = -\frac{1}{mr} A_g^\phi L_z, \quad (26)$$

and the quadratic gravitational potential in the  $x-y$  plane can be written as

$$\Phi_{m2} = \frac{1}{2} A_g^{\phi^2} = \frac{8\pi^2 \times 10^{-6}}{9} \frac{G^2}{c^2} f(r)^2. \quad (27)$$

The gravitational potentials  $\Phi$  (Eq. 20),  $\Phi_{m1}$  (Eq. 26) and  $\Phi_{m2}$  (Eq. 27) include some nontrivial integrals, which obscures their direct comparison. For clarity, we plot the gravitational potentials  $|\Phi|$ ,  $|\Phi_{m1}|$  and  $|\Phi_{m2}|$  in Fig. 2. We find  $\Phi$  to dominate over  $\Phi_{m1}$  and  $\Phi_{m2}$  in the  $x-y$  plane and thus that the latter two can be neglected.

The above introduction of angular momentum was based on a background soliton obeying Eq. (1), without rotation, that yields the density of the black curve in Fig. 1. The effect of rotation is modeled in Eq. (19) and has been shown to be negligible compared with the soliton's self-gravitating potential.

## B. Gravitomagnetic field due to a supermassive black hole spin

In this section, we consider the effect not only of the gravitoelectric field but also of the angular momentum from the central supermassive BH on a soliton rotating in a similar way as Sec. III A. In this case we express potentials in terms of a dimensionless distance in units of the Schwarzschild radius  $R_S = \frac{2GM_{bh}}{c^2}$ . To do so we define it for an arbitrary radial distance  $r$  as  $n = r/R_S$ . The gravitational potential sourced by a central supermassive BH follows

$$\Phi_e = -\frac{GM_{bh}}{r} = -\frac{c^2}{2n}. \quad (28)$$

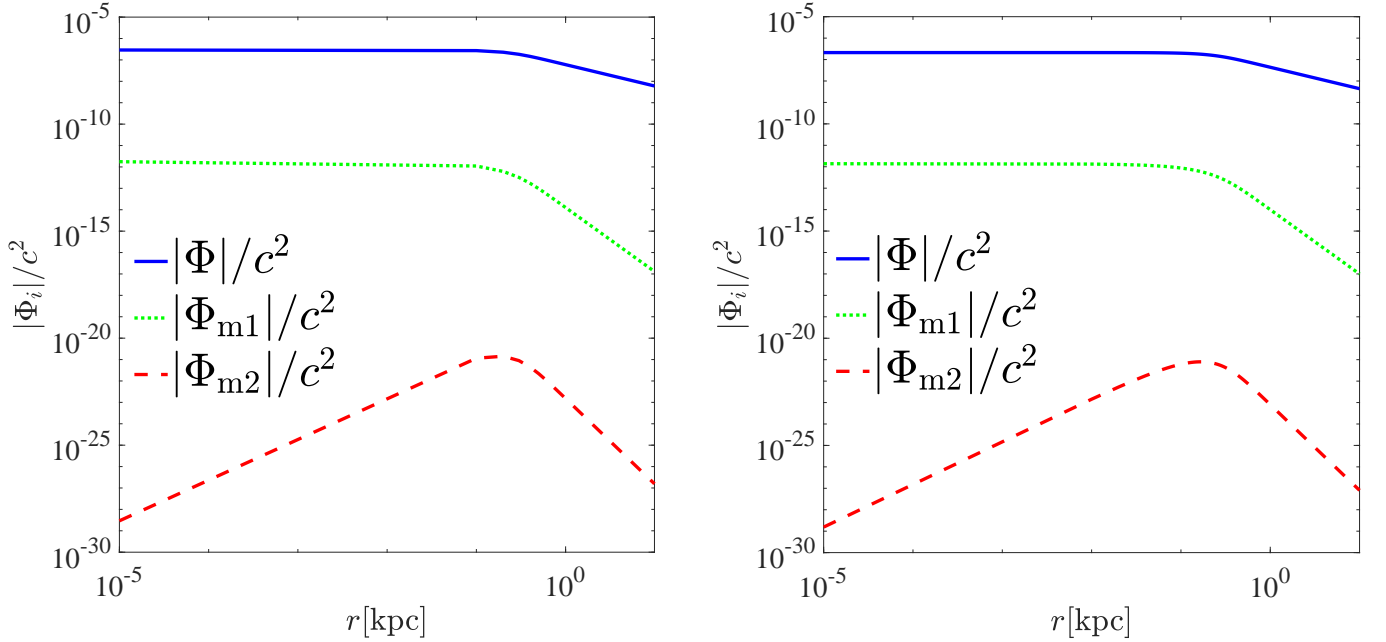


FIG. 2: Gravitational potentials  $|\Phi|$  (Eq. 20),  $|\Phi_{m1}|$  (Eq. 26) and  $|\Phi_{m2}|$  (Eq. 27) in the  $x - y$  plane, where the halo mass is similar to the Milky Way's,  $M_{\text{halo}} \approx 1 \times 10^{12} M_{\odot}$  [33], and the FDM particle has the typical mass  $m = 10^{-22} \text{eV}/c^2$ . In the left panel, we used the soliton-halo mass relation from Eq. (23), while the right panel used Eq. (24).

If this supermassive BH is spinning, the magnitude of its angular momentum is  $L_{\text{bh}} = \chi \frac{GM_{\text{bh}}^2}{c}$ , where  $\chi$  is a dimensionless spin parameter. According to gravitoelectromagnetism, the gravitomagnetic vector potential field  $\mathbf{A}_g$  depends on the angular momentum  $\mathbf{L}_{\text{bh}}$ , which points along the  $z$  direction, as

$$\mathbf{A}_g = -\frac{G}{2c^2 r^3} \mathbf{L}_{\text{bh}} \times \mathbf{r}. \quad (29)$$

The corresponding magnitude of the gravitomagnetic vector potential field  $A_g^\phi$  due to this spinning massive BH in the  $x - y$  plane reads

$$A_g^\phi = -\frac{G}{2c^2} \frac{L_{\text{bh}}}{r^2} = -\frac{\chi}{8n^2} c. \quad (30)$$

For an FDM particle, we can obtain its  $z$  direction angular momentum by Eq. (25), where  $v \sim 10^{-3}c$  and  $\rho$  is rescaled from the green curve in Fig. 1.  $\lambda$  is determined from the comparison between the integration of the green curve and  $M$  (Eq. 23 or 24). Meanwhile,  $M_{\text{bh}}$  is also rescaled from  $\tilde{M}_{\text{bh}} = 0.5$  with the same  $\lambda$ . According to Eq. (19), the linear gravitational potential in the  $x - y$  plane follows

$$\Phi_{m1} = -\frac{1}{mr} A_g^\phi L_z = \frac{1}{m} \frac{\chi}{8n^3} \frac{c}{R_S} L_z, \quad (31)$$

while the corresponding quadratic gravitational potential

writes

$$\Phi_{m2} = \frac{1}{2} A_g^{\phi 2} = \frac{\chi^2}{128n^4} c^2. \quad (32)$$

Comparing the gravitational potentials from Eqs. (28, 31 and 32), we find  $\Phi_e$  and  $\Phi_{m1}$  to dominate over  $\Phi_{m2}$  in the  $x - y$  plane and thus that the latter can be neglected for  $n \geq 1$  (outside the SMBH horizon). For clarity, we plot the gravitational potentials  $|\Phi_e|$ ,  $|\Phi_{m1}|$  and  $|\Phi_{m2}|$  in the  $x - y$  plane as a function of  $n$  in Fig. 3, where  $n \geq 1$  marks that the radial distance is larger than the Schwarzschild radius of the supermassive BH. We found that  $\Phi_{m1}$  is comparable to  $\Phi_e$  for radii within a decade of the Schwarzschild radius. According to Sec. II, this will further modify the soliton profile obtained from Eq. (2). Then, following Eq. (25), the angular momentum of the FDM particle should be affected, which in turn should modify  $\Phi_{m1}$  through Eq. (31). This loop reveals that our method cannot yield safely an evaluation of the potential for the gravitomagnetic field induced by the spin of a supermassive BH. To do so, the spherical symmetric approach of  $\Phi$  (Eq. 20) is insufficient to account for the cylindrical symmetric gravitomagnetic potential  $\Phi_{m1}$ . Solving the cylindrical symmetric system (Eq. 17) lies beyond the scope of the present paper.

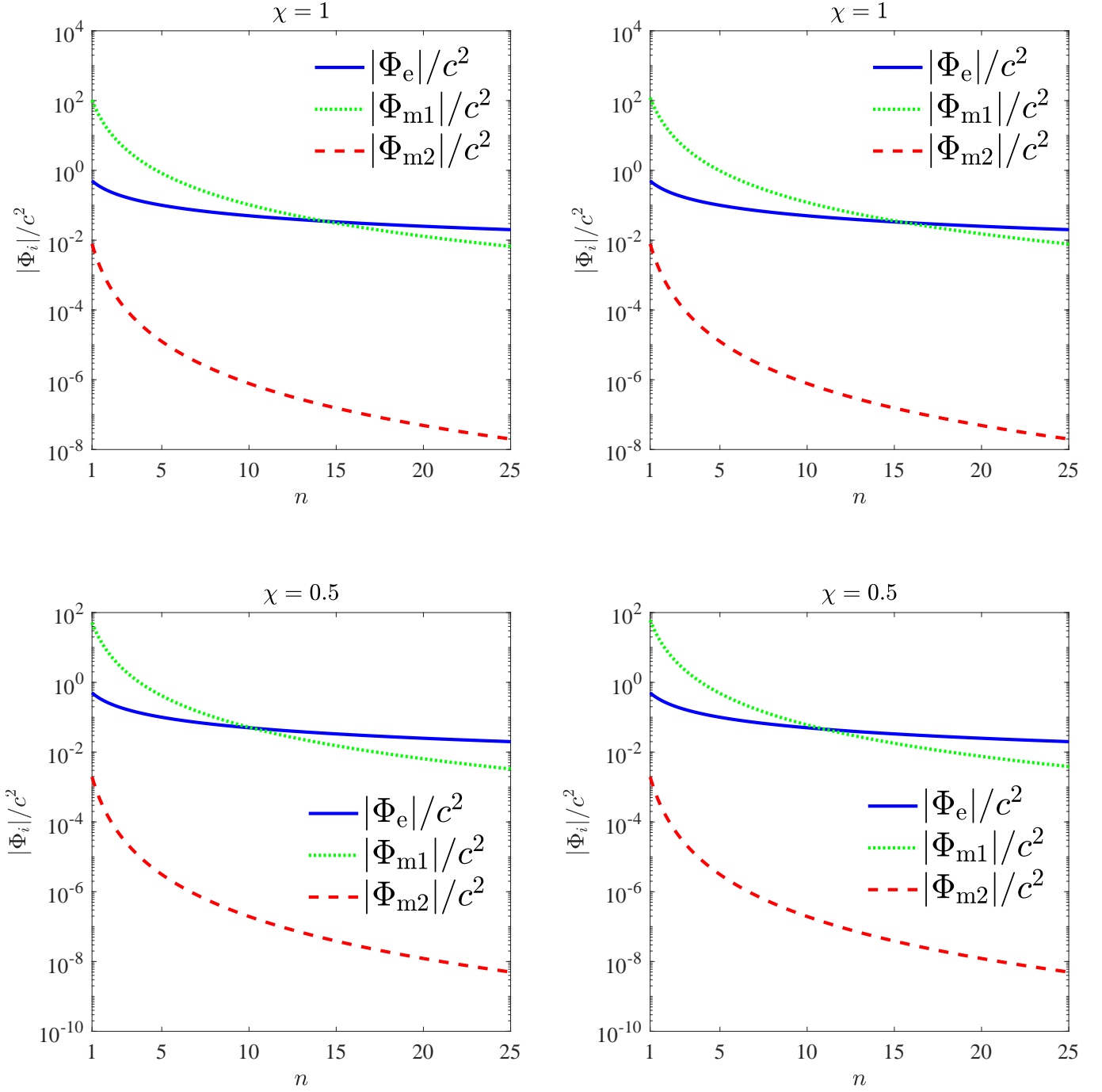


FIG. 3: Gravitational potentials  $|\Phi_e|$ ,  $|\Phi_{m1}|$  and  $|\Phi_{m2}|$  in the  $x - y$  plane as a function of  $n$  from Eqs. (28, 31 and 32) respectively, where  $n \geq 1$  marks that the radial distance is larger than the Schwarzschild radius of the supermassive BH. In the top subplots we set  $\chi = 1$  while in the bottom subplots,  $\chi = 0.5$ . Concomitantly, the left panels used the soliton-halo mass relation from Eq. (23), while the right panels used Eq. (24).

### C. Gravitomagnetic field due to the orbital motion of a supermassive black hole binary

In this section, we consider the effect not only of the gravitoelectric field but also of the angular momentum

from a supermassive BH binary on a soliton rotating in a similar way as Sec. III A. For simplicity, we consider an equal mass supermassive BH binary in a circular orbit in the  $x - y$  plane. These two supermassive BHs share the same mass  $M_{\text{bh}}$  and have a separation distance  $S = sR_S$

between each other, where  $s$  is a dimensionless parameter. The magnitude of the angular momentum for such binary is

$$L_{\text{bbh}} = I_{\text{bbh}} \Omega_{\text{bbh}} = \sqrt{s} \frac{GM_{\text{bh}}^2}{c}, \quad (33)$$

where the moment of inertia of this binary reduces to  $I_{\text{bbh}} = \frac{1}{2} M_{\text{bh}} S^2$  and its angular frequency follows  $\Omega_{\text{bbh}} = \frac{1}{\sqrt{s}} \frac{c}{S}$ . According to Eq. (29), the magnitude of the gravitomagnetic field due to this binary in the  $x - y$  plane yields

$$A_g^\phi = -\frac{G}{2c^2} \frac{L_{\text{bbh}}}{r^2} = -\frac{\sqrt{s}}{8n^2} c. \quad (34)$$

In addition, for an FDM particle, we can obtain its  $z$  direction angular momentum by Eq. (25), where  $v \sim 10^{-3}c$  and  $\rho$  is rescaled from the green curve in Fig. 1.  $\lambda$  is determined from the comparison between the integration of the green curve and  $M$  (Eq. 23 or 24). Meanwhile,  $2M_{\text{bh}}$  is also rescaled from  $\tilde{M}_{\text{bh}} = 0.5$  with the same  $\lambda$ . According to Eq. (19), the linear gravitational potential in the  $x - y$  plane follows

$$\Phi_{\text{m1}} = -\frac{1}{mr} A_g^\phi L_z = \frac{1}{m} \frac{\sqrt{s}}{8n^3} \frac{c}{R_S} L_z, \quad (35)$$

while the corresponding quadratic gravitational potential writes

$$\Phi_{\text{m2}} = \frac{1}{2} A_g^{\phi^2} = \frac{s}{128n^4} c^2. \quad (36)$$

We plot the gravitational potentials  $|\Phi_e| = \frac{c^2}{n}$ ,  $|\Phi_{\text{m1}}|$  (Eq. 35) and  $|\Phi_{\text{m2}}|$  (Eq. 36) in the  $x - y$  plane as a function of  $n$  in Fig. 4, where  $n \geq 1 + \frac{s}{2}$  marks that the radial distance is larger than the Schwarzschild radius of each supermassive BH plus half the binary separation,  $R_S + \frac{S}{2}$ . We found that  $\Phi_{\text{m1}}$  is comparable to  $\Phi_e$  for radii within a decade of the Schwarzschild radius. Similarly to subsec. IIIB, this will further modify the soliton profile obtained from Eq. (2). Then, following Eq. (25), the angular momentum of the FDM particle should be affected, which in turn should modify  $\Phi_{\text{m1}}$  through Eq. (35). Therefore, the spherical symmetric approach of  $\Phi$  (Eq. 20) is also insufficient to account for the cylindrical symmetric gravitomagnetic potential  $\Phi_{\text{m1}}$ .

#### IV. EFFECTS OF THE EXTREME DENSITY-RATIO SOLITON BINARY

The case of a system of two solitons, with density-ratio  $\sim 1$ , obviously does not feature spherical symmetry and could require numerical simulations [23–25]. On the contrary, the extreme case where the two solitons density-ratio  $\gtrsim 10^4$  presents two stages when this system do feature an approximate and local spherical symmetry: in stage 1) the higher density, smaller soliton lies

immersed within the boundary of the lower density, thus larger and relatively flatter, soliton which can be considered as a background; in stage 2) the lower density, larger soliton shares the same center as the higher density, smaller and more stable, soliton which can then be considered as a background. The collisional dynamics include these two stages and we can still use the shooting method to deal with them. Finally, we can use the exact SP system (Eq. 1) to describe the background soliton and the following variant of the exact SP system to describe the soliton with background in either of the above two stages

$$\begin{cases} i\hbar \frac{\partial \Psi}{\partial t} = \left( -\frac{\hbar^2}{2m} \nabla^2 + m\Phi \right) \Psi, \\ \nabla^2 \Phi = 4\pi G(|\Psi|^2 + \rho_{\text{bg}}), \end{cases} \quad (37)$$

whose dimensionless version is

$$\begin{cases} \frac{\partial^2(\tilde{r}\tilde{\psi})}{\partial \tilde{r}^2} = 2\tilde{r}(\tilde{\Phi} - \tilde{\gamma})\tilde{\psi}, \\ \frac{\partial^2(\tilde{r}\tilde{\Phi})}{\partial \tilde{r}^2} = \tilde{r}(\tilde{\psi}^2 + \tilde{\rho}_{\text{bg}}), \end{cases} \quad (38)$$

where  $\rho_{\text{bg}}$  is the density of the background soliton and its dimensionless counterpart is

$$\tilde{\rho}_{\text{bg}} \equiv \left( \frac{\hbar \sqrt{4\pi G}}{mc^2} \right)^2 \rho_{\text{bg}}. \quad (39)$$

Since this variant SP system (Eq. 38) also obeys the scaling symmetry when

$$\tilde{\rho}_{\text{bg}} \longrightarrow \lambda^2 \tilde{\rho}_{\text{bg}}, \quad (40)$$

we can choose to set up the background soliton with  $\lambda = 10^{-2}$  for stage 1 and with  $\lambda = 10^2$  for stage 2. Given the background density  $\rho_{\text{bg}}$ , the soliton with background can be found by solving Eq. (38) with the shooting method. By assuming that its density profile  $\tilde{\psi}^2(\tilde{r})$  can be different, while its dimensionless mass  $\tilde{M}$  remains fixed as the value listed in the first row of Tab. I, we get the eigenvalue  $\tilde{\gamma} = 0.6495$  for stage 1 and the eigenvalue  $\tilde{\gamma} = 69.2491$  for stage 2. The density profile  $\tilde{\psi}^2(\tilde{r})$  for each soliton is shown, for stage 1, in the left subplot, while it is shown, for stage 2, in the right subplot of Fig. 5. We find that the higher density, smaller soliton remains almost unaffected by the background soliton for stage 1 while the lower density, larger soliton shrinks dramatically for stage 2. After stage 2, two comparable solitons remain, corresponding to a smaller density-ratio case where numerical simulations could be required.

#### V. EFFECTS OF THE ELLIPSOIDAL BARYON PROFILE

Instead of a background soliton shown in section IV, we now consider a background baryon profile. More precisely, we consider an ellipsoidal baryon profile fitted on

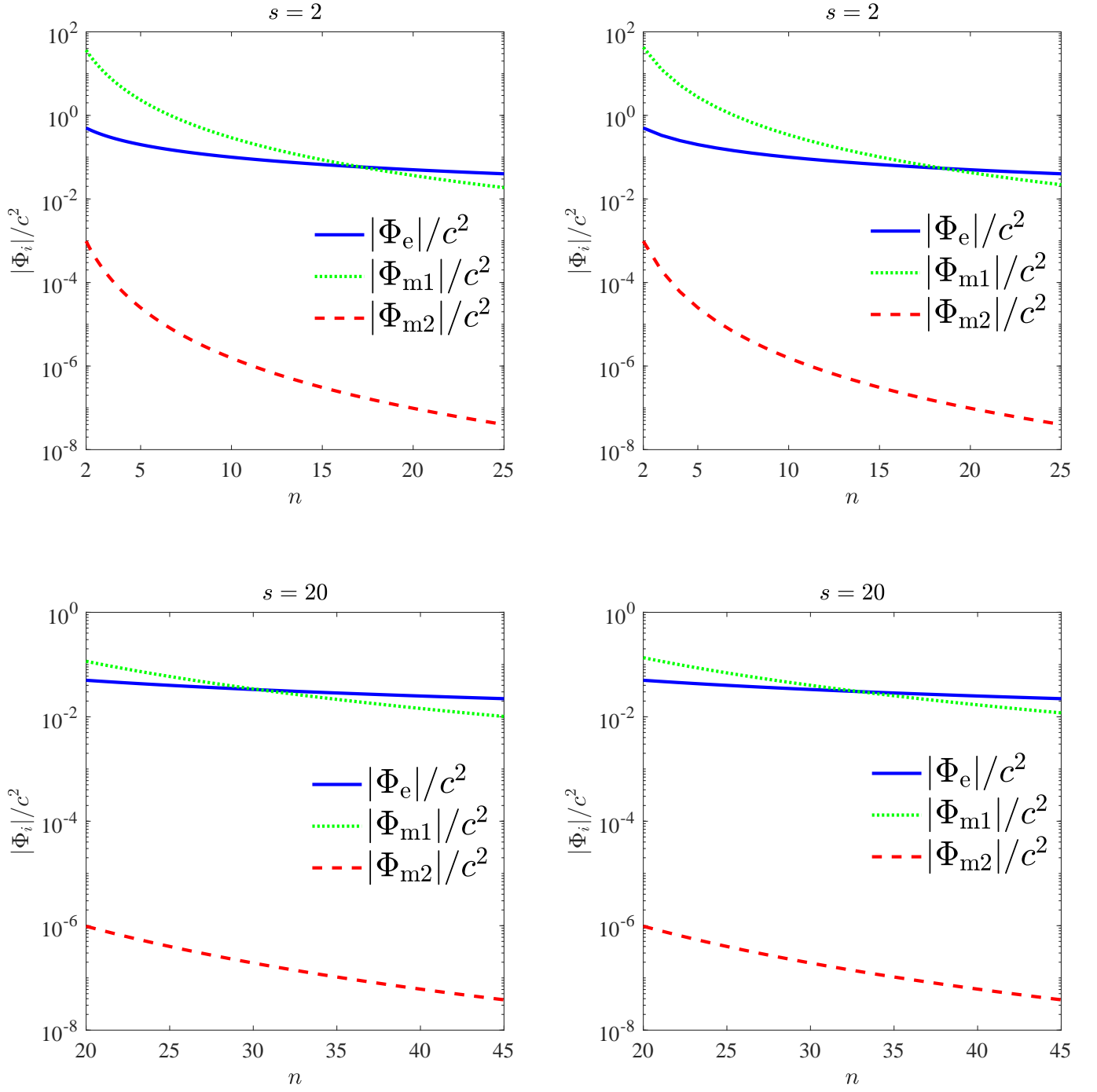


FIG. 4: Gravitational potentials  $|\Phi_e| = \frac{c^2}{n}$ ,  $|\Phi_{m1}|$  (Eq. 35) and  $|\Phi_{m2}|$  (Eq. 36) in the  $x - y$  plane as a function of  $n$ , where  $n \geq 1 + \frac{s}{2}$  marks that the radial distance is larger than the Schwarzschild radius of each supermassive BH plus half the binary separation,  $R_S + \frac{S}{2}$ . In the top subplots we set  $s = 2$  while in the bottom subplots,  $s = 20$ . Concomitantly, the left panels used the soliton-halo mass relation from Eq. (23), while the right panels used Eq. (24).

the Milky Way's [30, 31] three baryonic density components

$$\rho_{\text{bg}}(x, y, z) = \rho_{\text{bulge}}(x, y, z) + \rho_{\text{disk}}(x, y, z) + \rho_{\text{gas}}(x, y, z), \quad (41)$$

where  $\rho_{\text{bulge}}$  is a triaxial and bar-shaped bulge of stars at the inner few kpc of the Milky Way [34, 35],  $\rho_{\text{disk}}$  represents the galactic disk density profile and  $\rho_{\text{gas}}$  gives the diffuse gas component of the Milky Way which takes the form of molecular, atomic and ionised hydrogen and



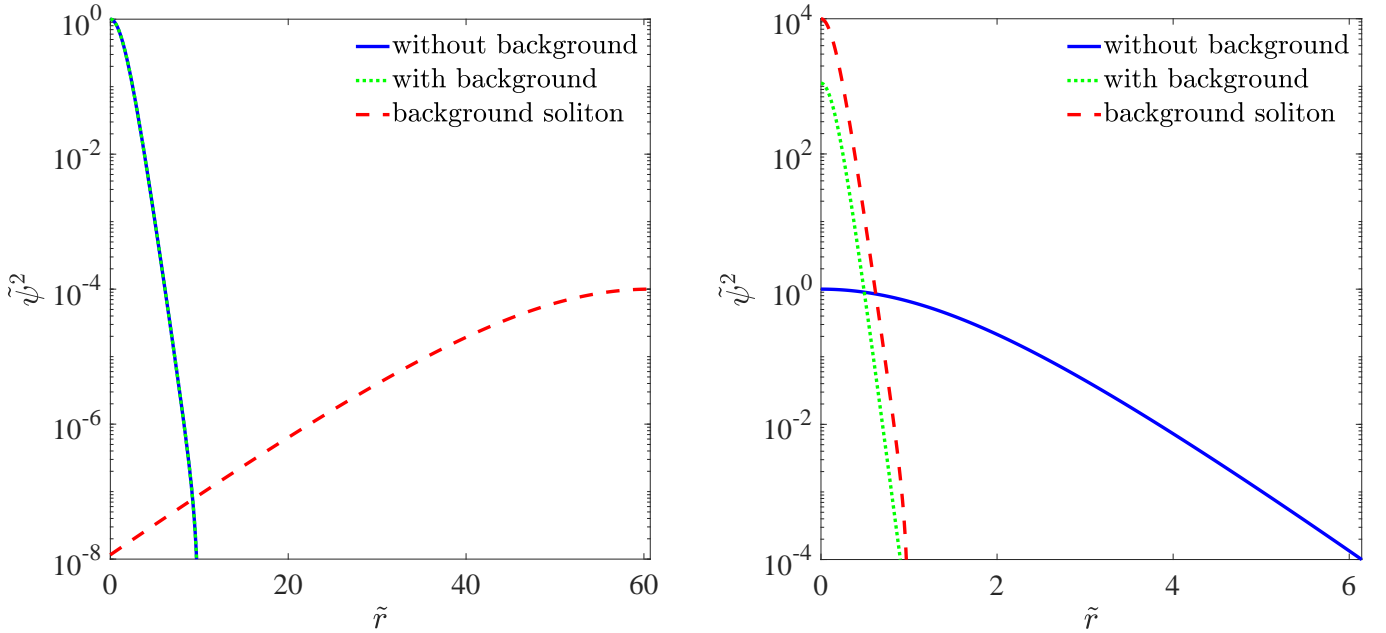


FIG. 5: Density profile  $\tilde{\psi}^2(\tilde{r})$  of each soliton for stage 1 (left) and stage 2 (right), for the case of Sec. IV.

heavier elements. The bulge can be fitted by

$$\rho_{\text{bulge}}(x, y, z) = 9.9 M_{\odot} \text{pc}^{-3} \times \exp \left\{ - \left[ x^2 + \left( \frac{y}{0.49} \right)^2 + \left( \frac{z}{0.37} \right)^2 \right]^{1/2} / 740 \text{pc} \right\}. \quad (42)$$

The disk density, because of its observed value  $\rho_{\text{disk}} \approx 0.05 M_{\odot} \text{pc}^{-3}$  [34], can be neglected compared with the bulge density. On the contrary, the diffuse gas density  $\rho_{\text{gas}}$ , is a non-negligible part of the baryons in the Milky Way. Here we assume that  $\rho_{\text{gas}} \approx m_{H_2} \langle n_{H_2} \rangle$ , where  $m_{H_2}$  is the mass of molecular hydrogen and  $\langle n_{H_2} \rangle$  is its number density in central molecular zone [36], fitted by

$$\langle n_{H_2} \rangle = 150 \text{cm}^{-3} \times \exp \left\{ - \left[ \frac{\sqrt{x^2 + (2.5y)^2} - 125 \text{pc}}{137 \text{pc}} \right]^4 \times \exp \left[ - \left( \frac{z}{18 \text{pc}} \right)^2 \right] \right\}. \quad (43)$$

For this non-spherical system, the shooting method fails and numerical simulations should be performed. However, we propose an approximation in which we consider three spherically averaged background baryon profiles respectively:  $\rho_{\text{bg}}^x(r) = \rho_{\text{bg}}(x = r, y = 0, z = 0)$ ,  $\rho_{\text{bg}}^y(r) = \rho_{\text{bg}}(x = 0, y = r, z = 0)$  and  $\rho_{\text{bg}}^z(r) = \rho_{\text{bg}}(x = 0, y = 0, z = r)$ . The shooting method can therefore be applied to these spherical approximations  $\rho_{\text{bg}}^i(r)$ . Should the results by each  $\rho_{\text{bg}}^i(r)$  be too markedly different, it would indicate that the original  $\rho_{\text{bg}}(x, y, z)$  is exceedingly non-spherical and unable to be described by the approximation  $\rho_{\text{bg}}^i(r)$ .

The way we find the equilibrium configurations, following the procedure of section II, uses an arbitrary normalization  $\tilde{\psi}(\tilde{r} = 0) = 1$  for which the normalized soliton mass  $\tilde{M} = \int_0^\infty \tilde{r}^2 \tilde{\psi}^2 d\tilde{r}$  deviates from the true dimensionless mass by a scaling factor  $\lambda$ . For the Milky Way, the soliton physical mass  $M \approx 1.25 \times 10^9 M_{\odot}$  or  $M \approx 1.16 \times 10^9 M_{\odot}$  is obtained with the soliton-halo mass relation Eq. (23) or (24). On the other hand, taking this scaling factor into consideration,  $\tilde{\rho}_{\text{bg}}^i \rightarrow \lambda^2 \tilde{\rho}_{\text{bg}}^i$  modifies the background baryon profile. To set both the soliton mass and the background baryon profile as the Milky Way's, we introduce an *a priori* scaling factor and obtain a new dimensionless variant as

$$\begin{cases} \frac{\partial^2(\tilde{r}\tilde{\psi})}{\partial \tilde{r}^2} = 2\tilde{r}(\tilde{\Phi} - \tilde{\gamma})\tilde{\psi}, \\ \frac{\partial^2(\tilde{r}\tilde{\Phi})}{\partial \tilde{r}^2} = \tilde{r}(\tilde{\psi}^2 + \lambda_0^{-2} \tilde{\rho}_{\text{bg}}^i), \end{cases} \quad (44)$$

where  $\lambda_0^{-2}$  is a parameter unaffected by the scaling factor  $\lambda$ , such that this system retains the scaling symmetry with  $\lambda_0^{-2} \tilde{\rho}_{\text{bg}}^i \rightarrow \lambda^2 \lambda_0^{-2} \tilde{\rho}_{\text{bg}}^i$ . Given an initial  $\lambda_0$ , we can obtain the normalized soliton profile  $\tilde{\psi}^2$ . The scaling factor  $\lambda$  can then be computed by requiring the soliton mass to be the Milky Way's. If  $\lambda/\lambda_0 \neq 1$ , we replace the initial  $\lambda_0$  with the computed  $\lambda$  and repeat the former two steps. We stop the iteration when  $\lambda/\lambda_0 - 1 < 0.0001$ .

In Tabs. II-VII, we list the eigenvalues  $\tilde{\gamma}$ , ground state solution soliton mass  $\tilde{M}$  and final value  $\lambda_0$  for each FDM mass  $m$ , background baryon profile  $\tilde{\rho}_{\text{bg}}^i$  and soliton physical mass  $M$ , respectively. We plot the normalized and the physical density profiles of the ground state solutions with different background baryon profile  $\tilde{\rho}_{\text{bg}}^i$  for various

FDM masses  $m$  and soliton physical masses  $M$  in Fig. 6 and Fig. 7, respectively. Comparing the soliton profiles corresponding to each  $\tilde{\rho}_{\text{bg}}^i$  in every subplot, we find that the fine-structure of the background baryon profile does not radically change the soliton profiles and that our treatment for the ellipsoidal baryon profile is reasonable. Contrasting the soliton profiles with different  $m$ , we find that heavier FDM particles form a denser, more compact and insensitive to the background baryon profile, soliton. Since, for the Milky Way, the soliton physical masses  $M$  derived from two soliton-halo mass relations Eqs. (23) and (24) are very similar, our results do not obviously depend on the choice of the soliton-halo mass relation.

TABLE II: Eigenvalue  $\tilde{\gamma}$ , ground state solution soliton mass  $\tilde{M}$  and final values  $\lambda_0$  for a set of FDM masses  $m$ , in the case of the background baryon profile  $\tilde{\rho}_{\text{bg}}^x$  and using the soliton-halo mass relation Eq. (23).

$m$	$\tilde{\gamma}$	$\tilde{M}$	$\lambda_0$
$1 \times 10^{-22} \text{eV}/c^2$	0.7600	1.4807	$4.3088 \times 10^{-7}$
$2 \times 10^{-22} \text{eV}/c^2$	0.7037	1.7103	$3.2300 \times 10^{-7}$
$5 \times 10^{-22} \text{eV}/c^2$	0.6644	1.9471	$2.4920 \times 10^{-7}$

TABLE III: Eigenvalue  $\tilde{\gamma}$ , ground state solution soliton mass  $\tilde{M}$  and final values  $\lambda_0$  for a set of FDM masses  $m$ , in the case of the background baryon profile  $\tilde{\rho}_{\text{bg}}^y$  and using the soliton-halo mass relation Eq. (23).

$m$	$\tilde{\gamma}$	$\tilde{M}$	$\lambda_0$
$1 \times 10^{-22} \text{eV}/c^2$	0.7521	1.6009	$3.6863 \times 10^{-7}$
$2 \times 10^{-22} \text{eV}/c^2$	0.7022	1.7670	$3.0256 \times 10^{-7}$
$5 \times 10^{-22} \text{eV}/c^2$	0.6642	1.9483	$2.4889 \times 10^{-7}$

TABLE IV: Eigenvalue  $\tilde{\gamma}$ , ground state solution soliton mass  $\tilde{M}$  and final values  $\lambda_0$  for a set of FDM masses  $m$ , in the case of the background baryon profile  $\tilde{\rho}_{\text{bg}}^z$  and using the soliton-halo mass relation Eq. (23).

$m$	$\tilde{\gamma}$	$\tilde{M}$	$\lambda_0$
$1 \times 10^{-22} \text{eV}/c^2$	0.7265	1.6652	$3.4068 \times 10^{-7}$
$2 \times 10^{-22} \text{eV}/c^2$	0.6859	1.8400	$2.7970 \times 10^{-7}$
$5 \times 10^{-22} \text{eV}/c^2$	0.6596	1.9922	$2.3805 \times 10^{-7}$

## VI. SUMMARY AND DISCUSSION

In this paper, we present reasonable variants of the exact SP system that predict FDM solitons in a non relativistic gravitational potential. Each variant aims at

TABLE V: Eigenvalue  $\tilde{\gamma}$ , ground state solution soliton mass  $\tilde{M}$  and final values  $\lambda_0$  for a set of FDM masses  $m$ , in the case of the background baryon profile  $\tilde{\rho}_{\text{bg}}^x$  and using the soliton-halo mass relation Eq. (24).

$m$	$\tilde{\gamma}$	$\tilde{M}$	$\lambda_0$
$1 \times 10^{-22} \text{eV}/c^2$	0.7773	1.4228	$3.9834 \times 10^{-7}$
$2 \times 10^{-22} \text{eV}/c^2$	0.6922	1.7784	$3.7065 \times 10^{-7}$
$5 \times 10^{-22} \text{eV}/c^2$	0.6537	2.0275	$4.6674 \times 10^{-7}$

TABLE VI: Eigenvalue  $\tilde{\gamma}$ , ground state solution soliton mass  $\tilde{M}$  and final values  $\lambda_0$  for a set of FDM masses  $m$ , in the case of the background baryon profile  $\tilde{\rho}_{\text{bg}}^y$  and using the soliton-halo mass relation Eq. (24).

$m$	$\tilde{\gamma}$	$\tilde{M}$	$\lambda_0$
$1 \times 10^{-22} \text{eV}/c^2$	0.7682	1.5464	$3.3721 \times 10^{-7}$
$2 \times 10^{-22} \text{eV}/c^2$	0.6898	1.8245	$3.5218 \times 10^{-7}$
$5 \times 10^{-22} \text{eV}/c^2$	0.6531	2.0265	$4.6720 \times 10^{-7}$

modeling a different effect, such as the variants due to a central supermassive BH (section II), the system's own angular momentum (section III), an extra denser and compact soliton (section IV) and an ellipsoidal baryon background (section V). We approximated each of them by an almost spherical system and solved them with the shooting method. We reach the same conclusion as [26], that the central supermassive BH renders the soliton denser and more compact. For the first time, we demonstrate that the effect of the gravitomagnetic field derived from the soliton's self-angular momentum can be neglected compared to the contributions from the soliton's self-gravitating field, while the effect of gravitomagnetic field derived from the central supermassive BH angular momentum is comparable to the contribution from the gravitoelectric field from that BH. Unlike the interference or collision of two similar solitons, certain snapshots of the interaction between two solitons with an extreme density-ratio is relatively simple: the smaller soliton with higher density is almost unaffected but the larger soliton with lower density shrinks dramati-

TABLE VII: Eigenvalue  $\tilde{\gamma}$ , ground state solution soliton mass  $\tilde{M}$  and final values  $\lambda_0$  for a set of FDM masses  $m$ , in the case of the background baryon profile  $\tilde{\rho}_{\text{bg}}^z$  and using the soliton-halo mass relation Eq. (24).

$m$	$\tilde{\gamma}$	$\tilde{M}$	$\lambda_0$
$1 \times 10^{-22} \text{eV}/c^2$	0.7395	1.6119	$3.1036 \times 10^{-7}$
$2 \times 10^{-22} \text{eV}/c^2$	0.6767	1.8899	$3.2823 \times 10^{-7}$
$5 \times 10^{-22} \text{eV}/c^2$	0.6523	2.0411	$4.6054 \times 10^{-7}$

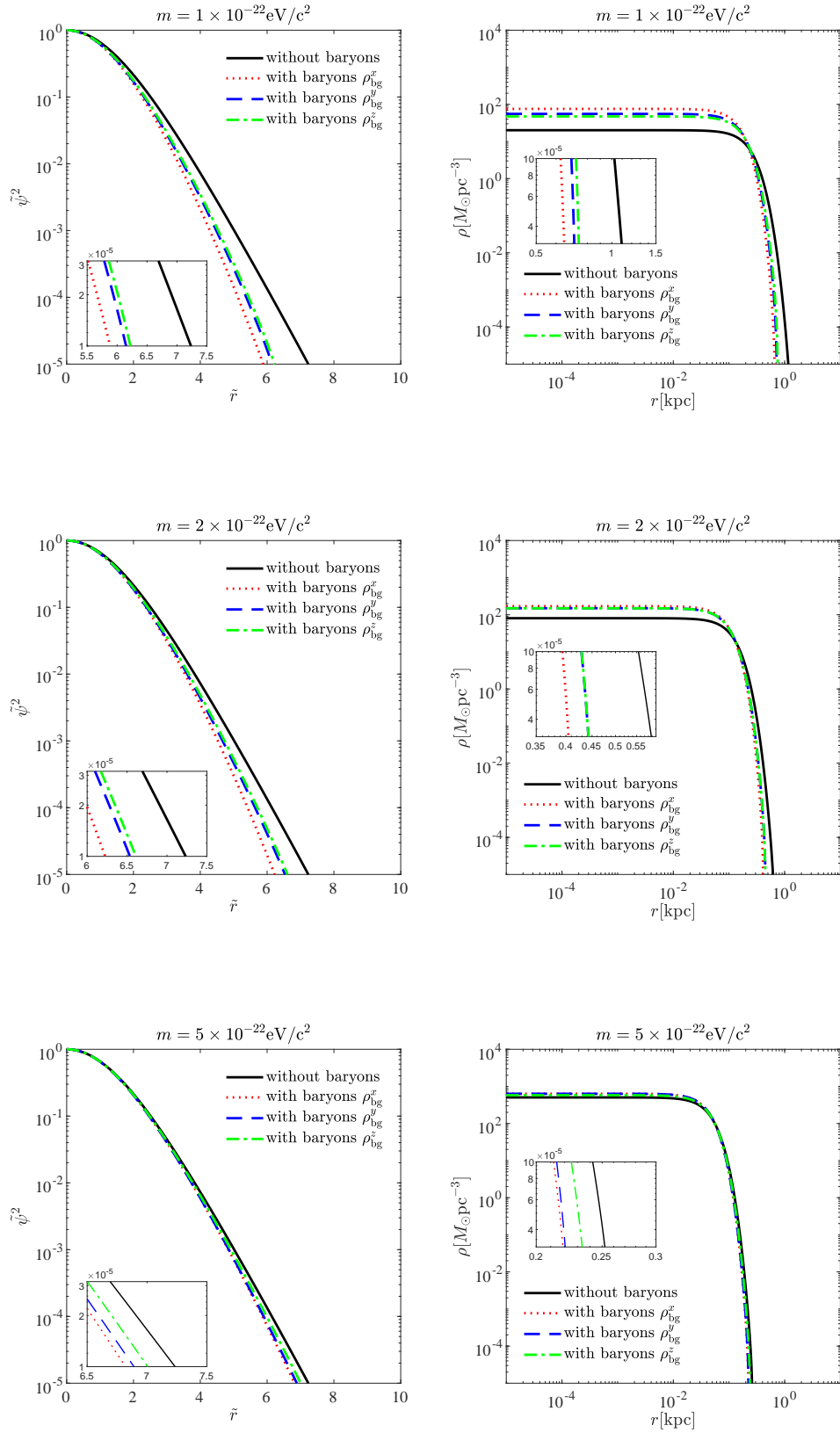


FIG. 6: Density profiles of the ground state solutions with different background baryon profile  $\tilde{\rho}_{\text{bg}}^i$  for various FDM masses  $m$  and using the soliton-halo mass relation Eq. (23): first row,  $m = 1 \times 10^{-22} \text{eV}/c^2$ , second row,  $m = 2 \times 10^{-22} \text{eV}/c^2$  and third row,  $m = 5 \times 10^{-22} \text{eV}/c^2$ ; first column gives normalized density profile while the second column represents the physical density profile; black curves mark pure FDM solitons without the background baryon profile, red dotted curves show the effect of  $\tilde{\rho}_{\text{bg}}^x$ , blue dashed curves, that of  $\tilde{\rho}_{\text{bg}}^y$  and green dash-dotted curves, of  $\tilde{\rho}_{\text{bg}}^z$ .

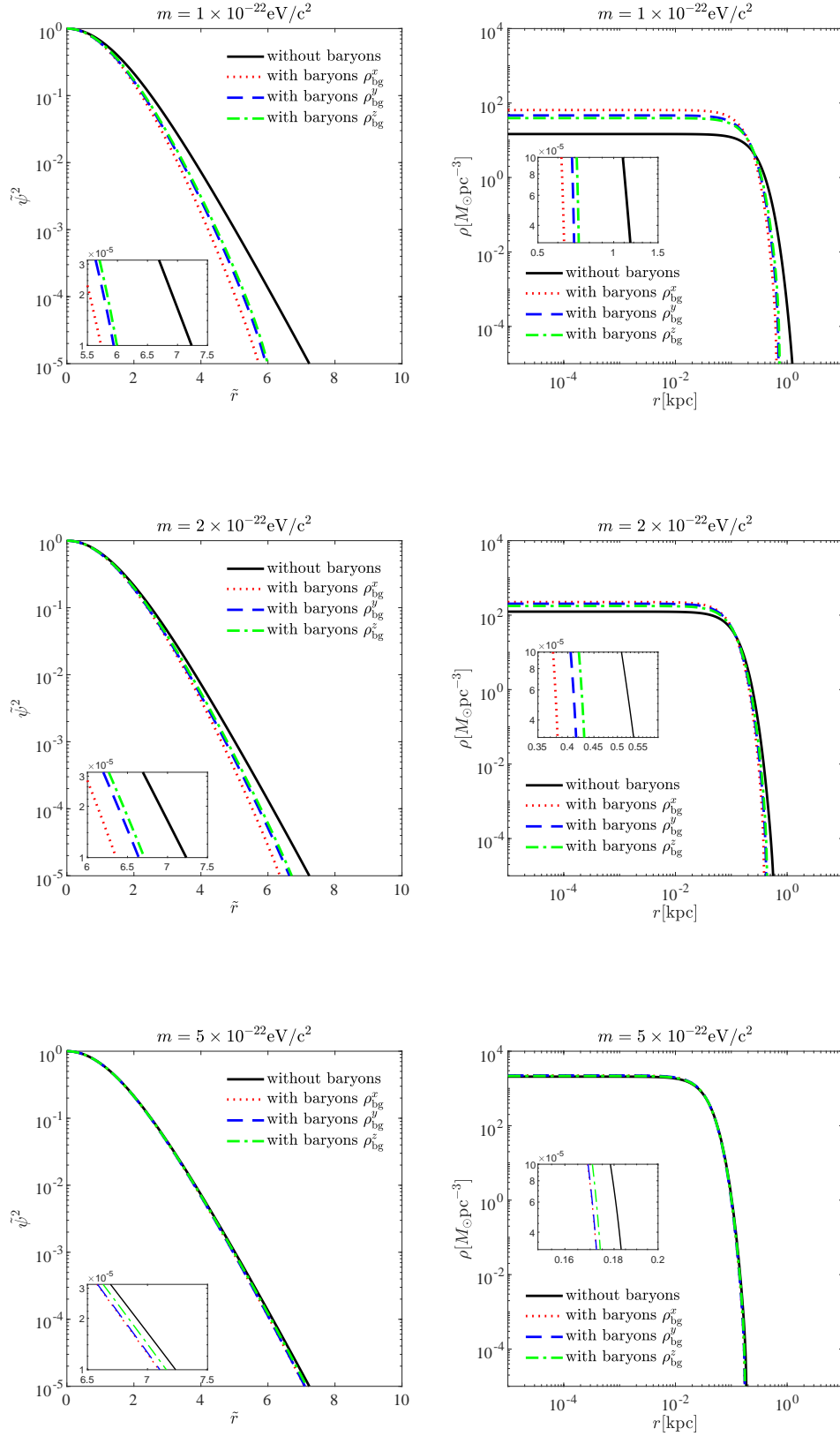


FIG. 7: Density profiles of the ground state solutions with different background baryon profile  $\tilde{\rho}_{\text{bg}}^i$  for various FDM masses  $m$  and using the soliton-halo mass relation Eq. (24): first row,  $m = 1 \times 10^{-22} \text{eV}/c^2$ , second row,  $m = 2 \times 10^{-22} \text{eV}/c^2$  and third row,  $m = 5 \times 10^{-22} \text{eV}/c^2$ ; first column gives normalized density profile while the second column represents the physical density profile; black curves mark pure FDM solitons without the background baryon profile, red dotted curves show the effect of  $\tilde{\rho}_{\text{bg}}^x$ , blue dashed curves, that of  $\tilde{\rho}_{\text{bg}}^y$  and green dash-dotted curves, of  $\tilde{\rho}_{\text{bg}}^z$ .

cally. Finally, we revisit the topic discussed in [29], showing that the baryon background is important for the soliton profile. We propose a reasonable treatment for the ellipsoidal baryon background, from which we are able to highlight the importance of the baryon background for lighter FDM particle.

Of course, we could enlarge the parameter space of the underlying theoretical model and produce a greater diversity in the soliton solution. For example, the self-interactions between FDM particles [37] or the modified gravitational potential due to the modified gravity [38] would result in a different set of coupled equations, hence a different soliton profile. In any case, the variants of the

exact SP system presented in this paper are taking into account environmental effects, so the mapping between a basic system and its variants should be common to theoretical models.

### Acknowledgments

MLeD acknowledges the financial support by the Lanzhou University starting fund, the Fundamental Research Funds for the Central Universities (Grant No. lzujbky-2019-25) and NSFC (grant No.12247101).

- 
- [1] V. C. Rubin, W. K. Ford, Jr., N. Thonnard and D. Burstein, “Rotational properties of 23 SB galaxies,” *Astrophys. J.* **261**, 439 (1982)
  - [2] M. Davis, G. Efstathiou, C. S. Frenk and S. D. M. White, “The Evolution of Large Scale Structure in a Universe Dominated by Cold Dark Matter,” *Astrophys. J.* **292**, 371-394 (1985)
  - [3] D. Clowe, M. Bradac, A. H. Gonzalez, M. Markevitch, S. W. Randall, C. Jones and D. Zaritsky, “A direct empirical proof of the existence of dark matter,” *Astrophys. J. Lett.* **648**, L109-L113 (2006) [arXiv:astro-ph/0608407 [astro-ph]].
  - [4] N. Aghanim *et al.* [Planck], “Planck 2018 results. VI. Cosmological parameters,” *Astron. Astrophys.* **641**, A6 (2020) [erratum: *Astron. Astrophys.* **652**, C4 (2021)] [arXiv:1807.06209 [astro-ph.CO]].
  - [5] R. H. Sanders, “Modified gravity without dark matter,” *Lect. Notes Phys.* **720**, 375-402 (2007) [arXiv:astro-ph/0601431 [astro-ph]].
  - [6] A. Tan *et al.* [PandaX-II], “Dark Matter Results from First 98.7 Days of Data from the PandaX-II Experiment,” *Phys. Rev. Lett.* **117**, no.12, 121303 (2016) [arXiv:1607.07400 [hep-ex]].
  - [7] D. S. Akerib *et al.* [LUX], “Improved Limits on Scattering of Weakly Interacting Massive Particles from Reanalysis of 2013 LUX Data,” *Phys. Rev. Lett.* **116**, no.16, 161301 (2016) [arXiv:1512.03506 [astro-ph.CO]].
  - [8] D. S. Akerib *et al.* [LUX], “Results from a search for dark matter in the complete LUX exposure,” *Phys. Rev. Lett.* **118**, no.2, 021303 (2017) [arXiv:1608.07648 [astro-ph.CO]].
  - [9] B. Carr, F. Kuhnel and M. Sandstad, “Primordial Black Holes as Dark Matter,” *Phys. Rev. D* **94**, no.8, 083504 (2016) [arXiv:1607.06077 [astro-ph.CO]].
  - [10] J. Primack, “Cosmology: small scale issues revisited,” *New J. Phys.* **11**, 105029 (2009) [arXiv:0909.2247 [astro-ph.CO]].
  - [11] P. Bull, Y. Akrami, J. Adamek, T. Baker, E. Bellini, J. Beltran Jimenez, E. Bentivegna, S. Camera, S. Clesse and J. H. Davis, *et al.* “Beyond  $\Lambda$ CDM: Problems, solutions, and the road ahead,” *Phys. Dark Univ.* **12**, 56-99 (2016) [arXiv:1512.05356 [astro-ph.CO]].
  - [12] W. Hu, R. Barkana and A. Gruzinov, “Cold and fuzzy dark matter,” *Phys. Rev. Lett.* **85**, 1158-1161 (2000) [arXiv:astro-ph/0003365 [astro-ph]].
  - [13] H. Y. Schive, T. Chiueh and T. Broadhurst, “Cosmic Structure as the Quantum Interference of a Coherent Dark Wave,” *Nature Phys.* **10**, 496-499 (2014) [arXiv:1406.6586 [astro-ph.GA]].
  - [14] H. Y. Schive, M. H. Liao, T. P. Woo, S. K. Wong, T. Chiueh, T. Broadhurst and W. Y. P. Hwang, “Understanding the Core-Halo Relation of Quantum Wave Dark Matter from 3D Simulations,” *Phys. Rev. Lett.* **113**, no.26, 261302 (2014) [arXiv:1407.7762 [astro-ph.GA]].
  - [15] I. De Martino, T. Broadhurst, S. H. Henry Tye, T. Chiueh, H. Y. Schive and R. Lazkoz, “Recognizing Axionic Dark Matter by Compton and de Broglie Scale Modulation of Pulsar Timing,” *Phys. Rev. Lett.* **119**, no.22, 221103 (2017) [arXiv:1705.04367 [astro-ph.CO]].
  - [16] P. Mocz, A. Fialkov, M. Vogelsberger, F. Becerra, M. A. Amin, S. Bose, M. Boylan-Kolchin, P. H. Chavanis, L. Hernquist and L. Lancaster, *et al.* “First star-forming structures in fuzzy cosmic filaments,” *Phys. Rev. Lett.* **123**, no.14, 141301 (2019) [arXiv:1910.01653 [astro-ph.GA]].
  - [17] D. J. Kaup, “Klein-Gordon Geon,” *Phys. Rev.* **172** (1968), 1331-1342
  - [18] R. Ruffini and S. Bonazzola, “Systems of self-gravitating particles in general relativity and the concept of an equation of state,” *Phys. Rev.* **187** (1969), 1767-1783
  - [19] T. X. Ma, C. Liang, J. Yang and Y. Q. Wang, “Hybrid Proca-boson stars,” *Phys. Rev. D* **108**, no.10, 104011 (2023) [arXiv:2304.08019 [gr-qc]].
  - [20] P. H. Chavanis, “Mass-radius relation of Newtonian self-gravitating Bose-Einstein condensates with short-range interactions: I. Analytical results,” *Phys. Rev. D* **84**, 043531 (2011) [arXiv:1103.2050 [astro-ph.CO]].
  - [21] P. H. Chavanis and L. Delfini, “Mass-radius relation of Newtonian self-gravitating Bose-Einstein condensates with short-range interactions: II. Numerical results,” *Phys. Rev. D* **84**, 043532 (2011) [arXiv:1103.2054 [astro-ph.CO]].
  - [22] F. S. Guzman and L. A. Urena-Lopez, “Evolution of the Schrodinger-Newton system for a selfgravitating scalar field,” *Phys. Rev. D* **69**, 124033 (2004) [arXiv:gr-qc/0404014 [gr-qc]].
  - [23] A. Paredes and H. Michinel, “Interference of Dark Matter Solitons and Galactic Offsets,” *Phys. Dark Univ.* **12**, 50-55 (2016) [arXiv:1512.05121 [astro-ph.CO]].
  - [24] F. Edwards, E. Kendall, S. Hotchkiss and R. East-

- her, “PyUltraLight: A Pseudo-Spectral Solver for Ultralight Dark Matter Dynamics,” *JCAP* **10**, 027 (2018) [arXiv:1807.04037 [astro-ph.CO]].
- [25] E. Munive-Villa, J. N. Lopez-Sanchez, A. A. Avilez-Lopez and F. S. Guzman, “Solving the Schrödinger-Poisson system using the coordinate adaptive moving mesh method,” *Phys. Rev. D* **105**, no.8, 083521 (2022) [arXiv:2203.10234 [gr-qc]].
- [26] E. Y. Davies and P. Mocz, “Fuzzy Dark Matter Soliton Cores around Supermassive Black Holes,” *Mon. Not. Roy. Astron. Soc.* **492**, no.4, 5721-5729 (2020) [arXiv:1908.04790 [astro-ph.GA]].
- [27] Ellis, G. F. R., Maartens, R., & MacCallum, M. A. H. 2012, “Relativistic Cosmology”, Cambridge, UK: Cambridge University Press, 2012
- [28] B. Salehian, H. Y. Zhang, M. A. Amin, D. I. Kaiser and M. H. Namjoo, “Beyond Schrödinger-Poisson: non-relativistic effective field theory for scalar dark matter,” *JHEP* **09**, 050 (2021) [arXiv:2104.10128 [astro-ph.CO]].
- [29] N. Bar, K. Blum, J. Eby and R. Sato, “Ultralight dark matter in disk galaxies,” *Phys. Rev. D* **99**, no.10, 103020 (2019) [arXiv:1903.03402 [astro-ph.CO]].
- [30] F. Iocco, M. Pato and G. Bertone, “Evidence for dark matter in the inner Milky Way,” *Nature Phys.* **11**, 245-248 (2015) [arXiv:1502.03821 [astro-ph.GA]].
- [31] H. N. Lin and X. Li, “The Dark Matter Profiles in the Milky Way,” *Mon. Not. Roy. Astron. Soc.* **487**, no.4, 5679-5684 (2019) [arXiv:1906.08419 [astro-ph.GA]].
- [32] H. Y. J. Chan, E. G. M. Ferreira, S. May, K. Hayashi and M. Chiba, “The diversity of core-halo structure in the fuzzy dark matter model,” *Mon. Not. Roy. Astron. Soc.* **511**, no.1, 943-952 (2022) [arXiv:2110.11882 [astro-ph.CO]].
- [33] W. Wang, J. Han, M. Cautun, Z. Li and M. N. Ishigaki, “The mass of our Milky Way,” *Sci. China Phys. Mech. Astron.* **63**, no.10, 109801 (2020) [arXiv:1912.02599 [astro-ph.GA]].
- [34] M. Lopez-Corredoira, A. Cabrera-Lavers and O. E. Gerhard, “A Boxy bulge in the Milky Way. Inversion of the stellar statistics equation with 2MASS data,” *Astron. Astrophys.* **439**, 107 (2005) [arXiv:astro-ph/0504608 [astro-ph]].
- [35] Y. H. Ryu, H. Y. Chang, M. G. Park and K. W. Lee, “Microlensing Optical Depth Revisited with Recent Star Counts,” *Astrophys. J.* **689**, 1078 (2008) [arXiv:0808.2539 [astro-ph]].
- [36] K. Ferriere, W. Gillard and P. Jean, “Spatial distribution of interstellar gas in the innermost 3 kpc of our Galaxy,” *Astron. Astrophys.* **467**, 611-627 (2007) [arXiv:astro-ph/0702532 [astro-ph]].
- [37] P. H. Chavanis, “Mass-radius relation of self-gravitating Bose-Einstein condensates with a central black hole,” *Eur. Phys. J. Plus* **134**, no.7, 352 (2019) [arXiv:1909.04709 [gr-qc]].
- [38] J. Chen and H. Y. Zhang, “Novel structures and collapse of solitons in nonminimally gravitating dark matter halos,” *JCAP* **10**, 005 (2024) [arXiv:2407.09265 [hep-ph]].